Inorganic Chemistry

Article

pubs.acs.org/IC

Vanadium Thiolate Complexes for Efficient and Selective Sulfoxidation Catalysis: A Mechanistic Investigation

Nikita Hall,[†,‡,§] Maylis Orio,*[,§,∥,⊥] Adeline Jorge-Robin,[†,#,¶] Béatrice Gennaro,[†,‡] Caroline Marchi-Delapierre,[†,#,¶] and Carole Duboc*[,†,‡,§]

[†]Univ Grenoble Alpes 38041 Grenoble Cedex 9, France

[‡]CNRS, UMR-5250 Département de Chimie Moléculaire, Laboratoire de Chimie Inorganique Redox, Institut de Chimie Moléculaire de Grenoble, FR-CNRS-2607, BP-53, 38041 Grenoble Cedex 9, France

[§]TGE Réseau National de RPE interdisciplinaire, FR-3443, 75231 Paris Cedex 05, France

[∥]Univ Lille Nord de France, UDSL, CNRS UMR 8516, BP 83, 59000 Lille, France

[⊥]Laboratoire de Spectrochimie Infrarouge et Raman, CNRS LASIR-UMR 8516, Bat C4 59655 Villeneuve d'Ascq Cedex, France

[#]CEA, iRTSV, LCBM, 38054 Grenoble, France

[¶]CNRS, UMR 5249, Grenoble, France

Supporting Information

ABSTRACT: The structural and electronic properties as well as the catalytic activity toward sulfoxidation of two new vanadium complexes have been investigated. They both possess in their coordination sphere two alkyl thiolate ligands: a dioxido V^V complex $[VO_2L^{NS2}](HNEt_3)$ (**1**) (L^{NS2} = 2,2′-(pyridine-2,6-diyl)bis(1,1′-diphenylethanethiol)) and an oxido V^{IV} complex $[VOL^{N2S2}]$ (**2**) (L^{N2S2} = 2,2′-(2,2′-bipyridine-6,6′-diyl)bis(1,1′-diphenylethanethiol)). The X-ray structure of **1** has revealed that the V^V metal ion is at the center of a distorted trigonal bipyramid. The optimized structure of **2** obtained by DFT calculations displays a square-pyramidal geometry, consistent with its EPR spectrum characterized by an axial $S = 1/2$ signal ($g_\perp = 1.988$, $g_\parallel = 1.966$, $A_{x(V)} = 45 \times 10^{-4}$ cm^{-1}, $A_{y(V)} = 42 \times 10^{-4}$ cm^{-1}, $A_{z(V)} = 135 \times 10^{-4}$ cm^{-1}). DFT calculations have shown that the HOMO (highest occupied molecular orbital) of **1** is notably localized on the two thiolate sulfur atoms (56% and 22%, respectively), consistent with the expected covalent character of the V^V−S bond. On the other hand, the SOMO (singly occupied molecular orbital) of **2** is exclusively localized at the V^{IV} ion (92%). Complexes **1** and **2** have shown an ability to catalytically oxidize sulfide into sulfoxide. The oxidation reactions have been carried out with thioanisole as substrate and hydrogen peroxide as oxidant. Yields of 80% and 75% have been obtained in 10 and 15 min for **1** and **2**, respectively. However, in terms of conversion, **1** is more efficient than **2** (81% and 44%, respectively). More importantly, the reaction is completely selective with no trace of sulfone produced. While **1** displays a poor stability, catalyst **2** shows the same efficiency after five successive additions of oxidant and substrate. The difference in reactivity and stability between both complexes has been rationalized through a mechanism study performed by means of experimental data (^{51}V NMR and EPR spectroscopy) combined with theoretical calculations. It has been shown that the structure of the *cis*-oxo peroxo V^V intermediate species, which is related to its stability, can partly explain these discrepancies.

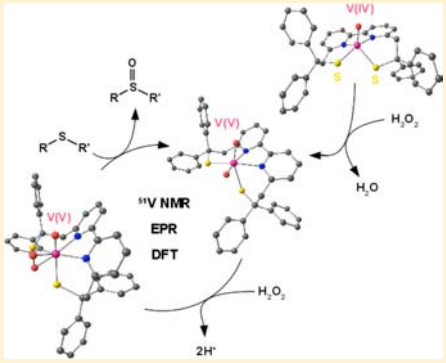

INTRODUCTION

A considerable amount of attention has been paid to vanadium coordination chemistry since the 1980s, when its presence in biological systems, its ability to catalyze oxidations and oxido transfer reactions, and also its prospective therapeutic applications were first demonstrated.[1−5] Vanadium is found in the active site of several metalloenzymes, for example in the V-dependent haloperoxidases that catalyze the halogenation of organic substrates and the oxidation of sulfides,[6,7] and in the V-containing nitrogenase that catalyzes the concomitant reduction of N_2 and H^+ into NH_4^+ and H_2.[8] Oxido vanadium(IV) and *cis*-dioxido vanadium(V) complexes with N- and O-donor chelating ligands have thus been studied as molecular models of the haloperoxidases.[1] These studies have revealed their great ability to catalytically oxidize various organic substrates, such as alkenes and aromatics, sulfides, and even alkanes, in the presence of hydrogen peroxide or alkyl hydroperoxides. Lastly, vanadium inhibits *in vivo* and *in vitro* the tyrosine phosphatase, inducing an insulin-enhancing effect.[9] In fact, oxido-vanadium(IV) and dioxido-vanadium(V) complexes with O-, N-, and S-based ligands have shown their capability to act as antidiabetic agents.[2] However, oxido V^{IV} compounds with alkyl thiolate ligands remain relatively uncommon with only a few being

Received: July 9, 2013
Published: November 13, 2013

   dx.doi.org/10.1021/ic4017504 | *Inorg. Chem.* 2013, 52, 13424−13431

characterized by X-ray diffraction experiments.[10−12] Furthermore, to the best of our knowledge, no structure has been reported so far for dioxido V^V complexes as far as alkyl thiolates are concerned. However, a few aromatic thiolate dioxido V^V complexes[13−15] and some mono-oxido aliphatic thiolate V^V compounds[16−19] have been reported to date. Yet, during the metabolism of the vanadium compounds, the metal could bind different types of biomolecules including cysteine or glutathione, which are alkyl thiolate S-based ligands. Recently, the controversial question of whether such thiolate derivates will or will not reduce high oxidation states of V has been clarified. A study has demonstrated that in physiological conditions, high stability of V^{IV} and even V^V complexes with thiolate ligands can be afforded depending on their redox potentials.[20]

The reactivity of oxido V^{IV} complexes with S-based ligands has been tested for different types of oxidation, especially sulfoxidation and epoxidation, with all the catalysts being synthesized with aromatic thiolate ligands (methyldithiocarbazate, dithiocarbonylhydrazone, and thiosemicarbazone).[21,22] These compounds present an activity comparable to that observed for O- and N-based ligands. Alkyl thiolate oxido V^{IV} complexes have also been recently investigated for their capability to perform S-alkylation reactions, but none for oxidation.[12]

Because we are interested in alkyl thiolate metal complexes, the work that we report herein is focused on potential applications of alkyl thiolate vanadium compounds for catalytic sulfoxidation using hydrogen peroxide as oxidant. In general, alkyl thiolates bound to a metallic ion are prone to generate sulfenic or sulfinic ligands in the presence of reactive oxygen species. In fact, in the active site of the nitrile hydratase enzymes, cysteine residues bound to the metal, either a Co^{III} or Fe^{III} ion, are oxidized.[23] In addition, it has been shown that peroxido-vanadium(V) complexes can oxidize thiols.[17,24] On the other hand, in Ni-superoxide dismutase, the cysteine residues bound to the Ni ion are stable in the presence of the superoxide radical anion substrate and the hydrogen peroxide product. In this context, it is of interest to test the potential of alkyl thiolate vanadium complexes for oxidation reactions.[25]

Two types of V compounds have been targeted, a very challenging dioxido V^V complex (**1**) and an oxido V^{IV} complex (**2**) (Scheme 1). Complex **2** has been synthesized using a N_2S_2 ligand (L^{N2S2}) that has previously been shown to generate quasi-square planar complexes with the Cu^{II},[26] Ni^{II},[27] Ni^{I},[28] and Zn^{II} ions,[29] and a square pyramidal complex with Fe^{III}.[30] To obtain the dioxido V^V complex, a tridentate ligand, L^{N2S}, has been used, previously described for the attainment of a Mo^{IV} complex.[31] In the present study, we report the synthesis and characterization of complexes **1** and **2** as well as their reactivity toward sulfoxidation. Furthermore, the electronic structure of both compounds has been explored by DFT calculations to investigate the effect of the thiolate especially on the nature of the V−S bond. Indeed, it has been shown that depending on the nature of the metal ion, high covalency of the M−S bond can be found, especially in the case of the Ni^{II} and Cu^{II} ions.[32] Curiously, as far as V^{IV} and V^V are concerned, such investigations have never been reported. Finally, we have explored the sulfoxidation mechanism by the use of both experimental techniques and theoretical calculations, with a special focus on the identification of intermediates in order to rationalize the difference in reactivity and stability observed between **1** and **2**.

Scheme 1

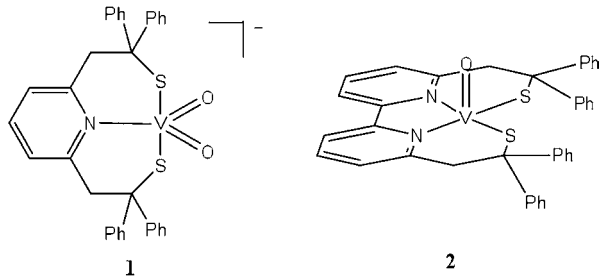

RESULTS

Synthesis and Description of the Molecular Structure of $[VO_2L^{NS2}](HNEt_3)$ (1) and $[VOL^{N2S2}]$ (2). The protonated L^{NS2} ligand (2,2′-(pyridine-2,6-diyl)bis(1,1′-diphenylethanethiol)) reacts in THF with VO_3NH_4 and NEt_3 leading to a yellow solution, which gives a yellow precipitate after one night under stirring, corresponding to $[VO_2L^{NS2}](HNEt_3)$(**1**). The potassium salt of the L^{N2S2} ligand (2,2′-(2,2′-bipyridine-6,6′-diyl)bis(1,1′-diphenylethanethiol)) reacts in THF with $VOSO_4$ leading to a light green precipitate corresponding to $[VOL^{N2S2}]$ (**2**). Both complexes are stable in air. Light orange crystals of **1** suitable for X-ray crystallography have been obtained from a solution of the reaction mixture on standing. Its molecular structure is presented in Figure 1, while selected bond distances and angles are listed in Table 1. The structure reveals an unprecedented dioxido V^V complex with two coordinated alkyl thiolate ligands. The structure consists of the $[VOL^{N2S2}]^-$ anion, one $HNEt_3^+$ cation, and one methanol solvent molecule. The V^V center of **1** is bound to the two aliphatic thiolates and to the pyridine unit of L^{NS2} in addition to two terminal oxido atoms, resulting in distorted trigonal bipyramidal coordination geometry around the metallic ion (τ = 0.78). The trigonal plane includes the two oxido oxygen atoms and the nitrogen atom of L^{NS2}. A value of 360° is calculated for the sum of the angles (range 110.03−127.19°) subtended at the metal ion, which is 0.013 Å out of this plane. The trigonal plane is notably distorted because the bonds to the terminal oxido ligands are significantly shorter (1.634 and 1.649 Å) than the V−N bond (2.197 Å). The sulfur atoms occupy the axial positions in a distorted fashion with a S−V−S angle of 157.08°. The V−S bond distances (2.406 and 2.410 Å) are notably longer than in the other oxido or dioxido vanadium(V) complexes (range 2.23−2.39 Å),[13−17] while the $V{=}O_{oxido}$ and V−N lengths are

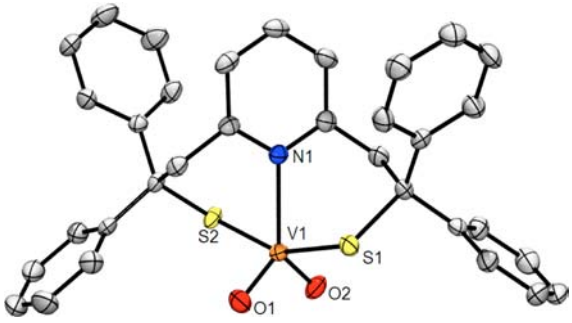

Figure 1. ORTEP diagram of $[VOL^{NS2}]^-$ (**1**$^-$). The thermal ellipsoids are drawn at 50% probability level. The hydrogen atoms have been omitted for clarity.

dx.doi.org/10.1021/ic4017504 | Inorg. Chem. 2013, 52, 13424−13431

Table 1. Selected Bond Lengths (Å) and Angles (deg) Issued from the X-ray Structure of 1 as well as from the DFT-Optimized Structures 1*·MeOH and 2*

	1, exptl	1*·MeOH, calcd		2*, calcd
V(1)–O(1)	1.633(2)	1.654	V(1)–O(1)	1.592
V(1)–O(2)	1.648(2)	1.636	V(1)–N(1)	2.340
V(1)–S(1)	2.4103(10)	2.455	V(1)–N(2)	2.343
V(1)–S(2)	2.4057(11)	2.433	V(1)–S(1)	2.192
V(1)–N(1)	2.197(2)	2.231	V(1)–S(2)	2.193
O(2)–H(1)	1.983	1.719		
O(1)–V(1)–O(2)	110.00(11)	112.7	N(1)–V(1)–N(2)	78.0
O(1)–V(1)–S(1)	91.67(8)	92.0	N(1)–V(1)–S(1)	95.3
O(1)–V(1)–S(2)	100.74(8)	100.3	N(1)–V(1)–S(2)	156.9
O(1)–V(1)–N(1)	122.76(10)	123.0	N(2)–V(1)–S(1)	166.7
O(2)–V(1)–S(1)	100.08(8)	102.2	N(2)–V(1)–S(2)	94.8
O(2)–V(1)–S(2)	93.72(8)	91.0	S(1)–V(1)–S(2)	86.9
O(2)–V(1)–N(1)	127.22(10)	124.2		
S(1)–V(1)–S(2)	157.09(3)	157.0		
S(1)–V(1)–N(1)	78.44(7)	78.7		

in the usual range. A strong intermolecular interaction is present via a hydrogen bond observed between the oxygen atom of an oxido ligand (O2) and the hydrogen atom of the alcohol function of the methanol molecule (2.105 Å).

An optimized geometry of **1** has been calculated by DFT and to obtain a fair agreement between both experimental and optimized structures, a methanol molecule has been included to account for the interaction with one oxido ligand via hydrogen bonding, as seen in the X-ray structure of **1**. The principal structural parameters of **1*·MeOH** (Table 1) reproduce well those of **1**, especially the V=O_{oxido} bond lengths. The calculated V–S/N distances are slightly longer (by ~4 pm) than the experimental ones (Table 1), which is typical for such optimization procedures.[33,34] Since this computational approach is reliable enough to predict the structure of this type of V compounds, DFT calculations were undertaken to optimize the geometry of complex **2** (Table 1). The resulting optimized structure (**2***) displays the expected square-pyramidal coordination geometry with the N_2S_2 donor set arranged around the basal plane and the vanadyl oxygen atom at the apex in agreement with EPR data (see below). The vanadium is displaced from the basal plane toward the apical oxygen atom by 0.28 Å. The V=O_{oxido} (1.592 Å) and V–S (2.340 and 2.343 Å) distances are within the ranges reported for N_2S_2 oxido vanadium(IV) complexes (1.58–1.63 and 2.34–2.37 Å, respectively).[10−12] Consequently, the calculated optimized structure **2*** is consistent with the structural data obtained on previously reported X-ray structures of dithiolate vanadyl complexes.

EPR Spectroscopy. EPR spectra of oxido vanadium(IV) complexes look essentially identical. They generally display an axial $S = 1/2$ signal consistent with a V^{IV} ion (d^1). Both transitions are split into eight lines due to the interaction between the unpaired electron and the ^{51}V (>99%) nuclear spin ($I = 7/2$).[35] The EPR spectrum of **2** recorded in a frozen CH_2Cl_2 solution at 100 K is shown in Figure 2. The spin Hamiltonian parameters used for the simulation are $g_\perp = 1.988$,

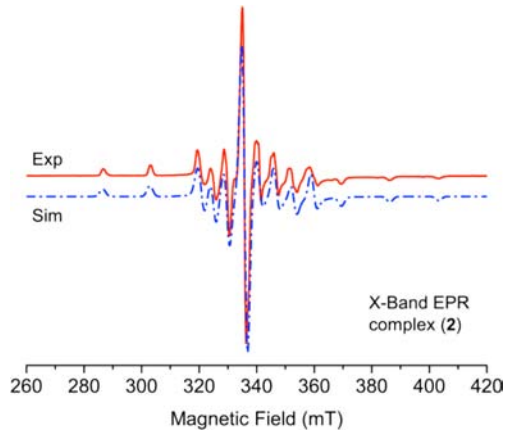

Figure 2. Experimental (red and solid line) and simulated (blue and dashed line) X-band EPR spectra of a solution of **2**. The parameters used for the simulation are given in the text.

$g_\parallel = 1.966$, $A_{x(V)} = 45 \times 10^{-4}$ cm^{-1}, $A_{y(V)} = 42 \times 10^{-4}$ cm^{-1}, $A_{z(V)} = 135 \times 10^{-4}$ cm^{-1}. These EPR parameters are typical of square pyramidal oxido vanadium(IV) complexes under comparable sulfur-containing donor environments with notable small A values.[12,14,36,37] The calculated EPR parameters ($g_x = 1.991$, $g_y = 1.985$, $g_z = 1.969$, $A_{x(V)} = -34 \times 10^{-4}$ cm^{-1}, $A_{y(V)} = -36 \times 10^{-4}$ cm^{-1}, $A_{z(V)} = -135 \times 10^{-4}$ cm^{-1}) obtained with the optimized **2*** structure are consistent with the experimental data, demonstrating that the geometry of **2** is retained in solution.

Electronic Structure. Complex **1** is a diamagnetic complex, V^V being a d^0 ion. The HOMO (highest occupied molecular orbital) of **1** presented in Figure 3 is notably localized on the

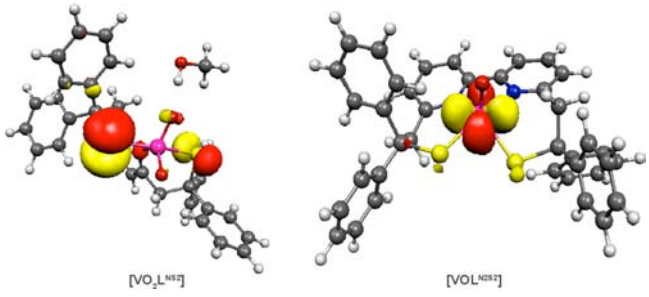

Figure 3. HOMO (left) and localized SOMO (right) for the complexes **1** and **2**. Color scheme: V, pink; S, yellow; O, red; N, blue; C, gray; H, white.

two thiolate sulfur atoms (56% and 22%, respectively), in accordance with the expected strong ionic character of the V^V–S bond as it was observed for the Zn^{II}–S bond in thiolate Zn^{II} compounds. Conversely, the SOMO (singly occupied molecular orbital) of complex **2** is exclusively localized on the V^{IV} ion (92%), the contribution of the sulfur atoms representing only 4% of the SOMO (Figure 3). Generally, the SOMO of vanadyl complexes is a metal-based orbital with a main d_{xy} character, as in **2**, where the x- and y-axes are seen to lie approximately along the σ bonds of the equatorial ligands. This orbital is largely nonbonding or participates in in-plane π bonding with ligand orbitals of correct symmetry. In the present case, the sulfur or

dx.doi.org/10.1021/ic4017504 | Inorg. Chem. 2013, 52, 13424–13431

nitrogen atoms do not contribute to the SOMO explaining the quasi-pure metal-based character of the SOMO in **2**. This is confirmed by the Mulliken population analysis showing that the metal bears all of the spin density with positive spin population (1.19) found at the V center. Such electronic properties notably differ from those observed with other metallic ions, such as Fe^{II}, Co^{II}, Ni^{II}, or Cu^{II}, coordinated to thiolate ligands,[32,38] obviously due to the electronic configuration of the metal (d^1 ion) determining the specific nature of the SOMO (d_{xy}) in vanadyl complexes. For example, the SOMO of the low-spin Ni^{III} complex synthesized with L^{N2S2}, presenting the same square based pyramidal geometry as **2**, was also a metal-based orbital but with a main d_{z^2} character and a lesser contribution of the metal (76%).[27] The absence of thiolate contribution to the SOMO is in accordance with the low S-alkylation reactivity of a previously described vanadyl complex with a mixed amine/thiolate ligand.[12]

Catalytic Sulfoxidation. The oxidation reactions have been carried out with methylphenylsulfide (thioanisole) used as a model substrate and hydrogen peroxide (H_2O_2) as oxidant, in CH_3CN and CH_2Cl_2/CH_3CN (1:1) for **1** and **2**, respectively. Scheme 2 represents the formation of the two expected

Scheme 2

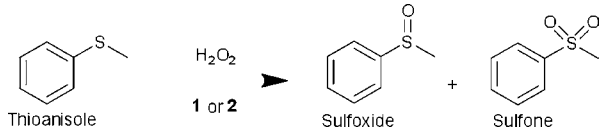

oxidation products (sulfoxide and sulfone). Table 2 summarizes the principal results obtained. The catalysts have been tested under two different conditions, that is, in both cases the concentration of catalyst and thioanisole was kept at 1 mM and 100 mM, respectively, while two concentrations in H_2O_2 have been tested (20 and 100 mM).

Both thiolate vanadium complexes have proven to be excellent for catalyzing sulfoxidation with yields up to 80%. More importantly, the reaction is very selective with no trace of sulfone produced under all conditions with both catalysts. The kinetics data performed with the 1/20/100 ratio for catalyst/H_2O_2/substrate show that the reaction is complete after 10 and 15 min with **1** and **2**, respectively (Figure 4). Catalyst **1** displays slightly better performance with 17 TON versus 15 TON for **2**.

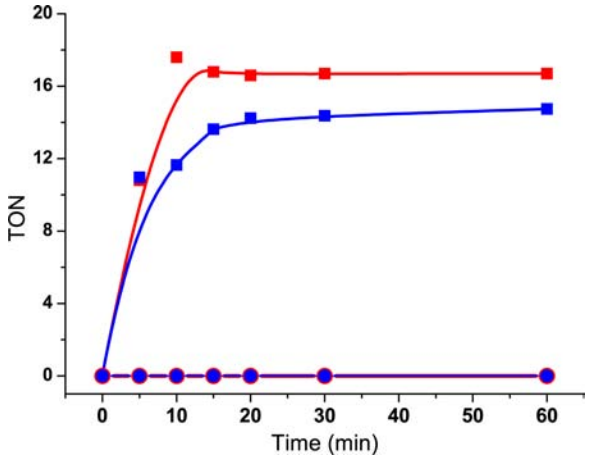

Figure 4. Turnover number (TON) of sulfoxide (■) and sulfone (●) produced from thioanisole (100 mM) with **1** (1 mM, red) or **2** (1 mM, blue) after the addition of H_2O_2 (20 mM).

The same experiments have been carried out in the presence of air, and similar results have been obtained, demonstrating that O_2 has no effect on the reactivity of both catalysts. This finding, in addition to the selectivity of the reaction toward sulfoxide, is consistent with a S_N2 mechanism via a heterolytic pathway, which is generally observed for vanadium catalysts.[1]

Quantitative catalytic experiments with the 1/100/100 ratio for catalyst/H_2O_2/substrate have been carried out to test the efficiency of the catalysts in terms of conversion. While catalyst **1** presents the same efficiency as found when using 20 equiv of H_2O_2 with a yield (or conversion) of 81%, the reactivity of catalyst **2** is sensitive to the oxidant/substrate ratio with a notable decrease of the yield to 45% when this ratio increases.

The stability of both catalysts has been investigated. In the case of catalyst **1**, when 20 equiv of H_2O_2 is added after a first run, neither additional sulfoxide nor sulfone is produced, demonstrating that the catalyst is completely degraded. On the other hand, after five successive additions of 20 equiv of H_2O_2 every 20 min (Figure 5), catalyst **2** is still active but with a steady decrease of its efficiency. Because we have already observed that the reactivity of **2** is sensitive to the oxidant/substrate ratio, another experiment in which this ratio is kept the same has been performed. After five successive additions of 20 equiv of H_2O_2 and 100 equiv of thioanisole every 20 min,

Table 2. Sulfoxidation of Thioanisole Using 1 and 2 as Catalysts and H_2O_2 as Oxidant Compared with the Reactivity of Other Vanadium Based Catalysts Reported in the Literature

catalyst	ratio[a]	yield (%)[b]	time (min)	TON[c]	SO/SO_2[d]	ref
1	1/100/20	80	10	17	100/0	this work
2	1/100/20	75	15	15	100/0	this work
1	1/100/100	81	≤ 30	81	100/0	this work
2	1/100/100	45	≤ 30	45	100/0	this work
$[VO(L^{NO3})]$[e]	1/100/100	97	25	97	96/4	40
$[VO(L^{NO3})]$[e]	0.1/100/100	98	80	980	98/2	40
$[VO(L^{NO3})]$[e]	0.01/100/100	97	850	9700	97/3	40
[VO(pydx-1,3-pn)][f]	0.02/100/100	79	150	2290	81/19	41
[VO(tmbmz)2]$^{-}$[g]	0.1/100/100	82	180	738	90/10	39
$[VO(L^{N2O2})Cl]$[h]	1/100/100	78	240	78	97/3	42

[a]Catalyst/substrate/oxidant ratio. [b]Yield based on the oxidant. [c]TON, moles of product per mole of V catalyst. [d]Sulfoxide/sulfone ratio. [e]L^{NO3}, a tetradentate NO_3 donor ligand. [f]pydx-1,3-pn, a tetradentate N_2O_2 donor ligand. [g]H_2tmbmz, 2-mercaptomethylbenzimidazole. [h]L^{N2O2}, a tetradentate N_2O_2 donor ligand.

dx.doi.org/10.1021/ic4017504 | Inorg. Chem. 2013, 52, 13424−13431

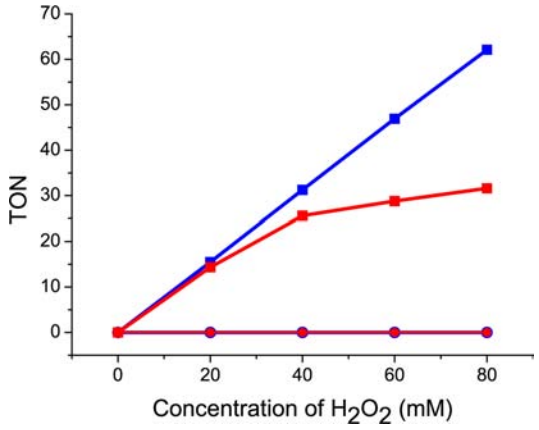

Figure 5. Turnover number (TON) of sulfoxide (■) and sulfone (●) produced using **2** (1 mM) as catalyst after successive additions every 20 min of 20 equiv of H_2O_2 in a solution containing thiolanisole (100 equiv, red) or of 20 equiv of H_2O_2 + 100 equiv of thioanisole (blue).

catalyst **2** displays the same efficiency and selectivity with respect to the first run, evidencing a remarkable stability (Figure 5).

Comparison with Literature. Both systems that contain alkyl thiolate ligands are the first vanadium catalysts reported to date toward sulfoxidation. To the best of our knowledge, the only vanadium−sulfur complex that has been previously studied for sulfoxidation contains aromatic thiolate ligands.[39] As an example, when 0.1 mol % of $[VO(tmbmz)_2]^-$ is used as catalyst with a thioanisole/H_2O_2 ratio of 1/1, the catalyst achieves 82% conversion with 10% sulfone production in 3 h (Table 2).

The results obtained with catalysts **1** and **2** are comparable to those found for the more common vanadium-based catalysts, which contain O- and N-based ligands in similar coordination (see Table 2 for examples). By far the most efficient catalyst is that reported by Mba et al.,[40] which presents a TON up to 9700 with only 3% production of sulfone in 14 h. However, to obtain such a large TON, low catalyst loadings are needed (≤0.1%), with a 1:1 ratio between thioanisole and H_2O_2. The only potential problem with these conditions is a decrease in the selectivity of the reaction. As an example, with catalyst [VO(pydx-1,3-pn)], a high production of sulfone (19%) is observed with a very low (0.1%) catalyst loading.[41]

In the case of **1** and **2**, such a high excess of H_2O_2 with respect to the catalyst concentration cannot be used due to the reactivity of the alkyl thiolates. Furthermore, as already mentioned, the increase of the H_2O_2/thioanisole ratio leads to a decrease in efficiency with **2**. However, as shown by the stability study, higher TONs are able to be achieved by successive additions of H_2O_2 and thioanisole.

Both catalysts $[VO(L^{NO3})]$[40] and $[VO(L^{N2O2})Cl]$[42] have been run under similar conditions to our studies (catalyst/H_2O_2/thioanisole ratio, 1/100/100) and show comparable results to catalysts **1** and **2** (Table 2). Consequently, it can be concluded that with both catalysts **1** and **2** the sulfoxidation is very rapid for vanadium-based catalysts. In addition, their main advantage is their complete selectivity toward the production of sulfoxide.

Mechanistic Investigation. From the above study concerning the reactivity of both complexes **1** and **2**, we can conclude that although **2** has a lower efficiency with respect to **1**, catalyst **2** displays significantly higher stability. To investigate these differences, we have carried out experiments in order to further investigate the mechanism.

Scheme 3 is adapted from the generally accepted catalytic cycle proposed for sulfoxidation by vanadium(IV) or (V)

Scheme 3

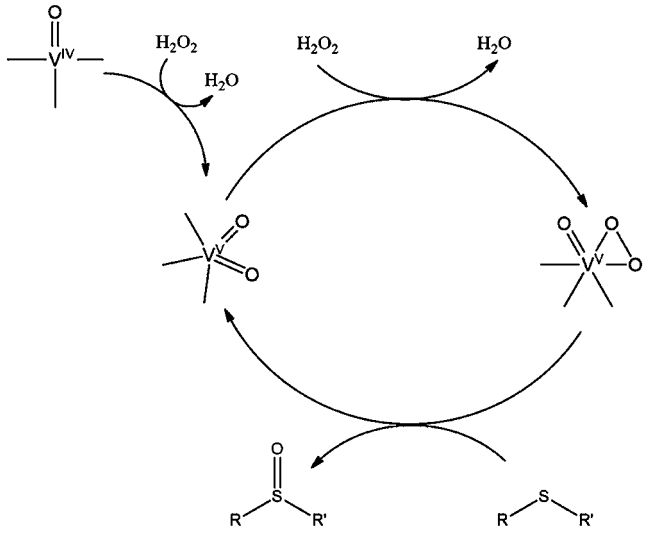

complexes.[41,43] The commonly proposed active species is a *cis*-oxido peroxido vanadium(V) intermediate. Consequently, when considering V^{IV} complexes, the activating step corresponds to their oxidation into V^V species, which will correspond to the "real" catalysts.

Looking first at catalyst **2**, the reaction has been followed by EPR spectroscopy. First no change in the EPR spectrum has been observed when thioanisole (100 equiv vs **2**) is added, in agreement with the fact that the reaction does not involve the coordination of the substrate on the V center. Second, after the addition of H_2O_2 (20 equiv), the EPR spectrum became silent, consistent with the oxidation of **2** into a diamagnetic V^V species. We also used ^{51}V NMR to investigate the catalytic cycle. While no peak is observed with the initial solutions, as soon as the oxidant is added, a peak appears at −707 ppm. After 1 h, a decrease of this peak and concomitant formation of a new peak at −555 ppm is observed. Based on the mechanism shown in Scheme 3, the −707 ppm peak can be attributed to a peroxido V^V intermediate, while that at −555 ppm can be attributed to the active catalyst related to **2**, which corresponds to a V^V species.

For catalyst **1**, the reaction has been followed by ^{51}V NMR only. The initial spectrum displays a signal at −389 ppm, which is insensitive to the addition of thioanisole. After the addition of H_2O_2, this peak instantaneously disappears with the concomitant appearance of three peaks at 603, 611, and 618 ppm (relative intensity, 1/2/1), the intensity of which remains the same for the next 12 h. Based on the fact that catalyst **1** is completely inactive after one run, we attribute these peaks to degraded form(s) of **1**.

Based on these data, a computational investigation has been carried out in order to better describe the active species of catalysts **1** and **2** and also with the aim of providing information to rationalize their differences in reactivity and stability. Three different structures displayed in Figure 6 have been optimized: (i) the catalytically active form of **2**, $[V(O)_2L^{N2S2}]^-$ ($\mathbf{2}^{(O)2}$), (ii) the oxido peroxido vanadium(V) complex derived from **2**,

dx.doi.org/10.1021/ic4017504 | *Inorg. Chem.* 2013, 52, 13424−13431

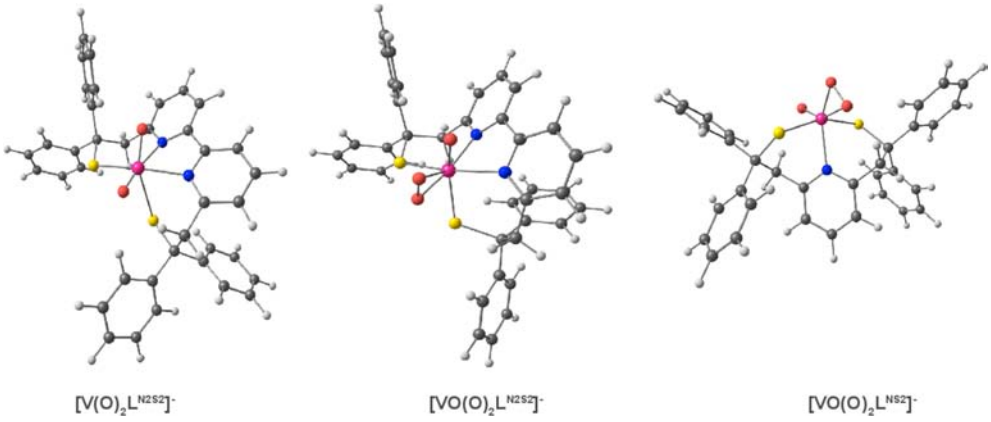

Figure 6. DFT optimized structures of $\mathbf{2}^{(O)2}$, $\mathbf{2}^{O(O2)}$, and $\mathbf{1}^{O(O2)}$. Color scheme: V, pink; S, yellow; O, red; N, blue; C, gray; H, white.

$[VO(O_2)L^{N2S2}]^-$ ($\mathbf{2}^{O(O2)}$), and (iii) the oxido peroxido vanadium(V) complex derived from **1**, $[VO(O_2)L^{NS2}]^-$ ($\mathbf{1}^{O(O2)}$).

The DFT-calculated ^{51}V NMR shifts have been predicted for these models, and the values are reported in Table 3. They are all in the expected range for such complexes. In fact, the $\delta(^{51}V)$ range for complexes with only O-, N- or S-based ligands is extremely broad, between +600 to −600 ppm. In addition, the $\delta(^{51}V)$ is mainly affected by ligands with large electronegativity values such as oxido ligands, while variations of the coordination number between 4 and 6 do not influence NMR chemical shifts significantly.[44,45] Consequently, the exchange of an oxido ligand by a peroxido one should lead to a more negative $\delta(^{51}V)$ as it has been previously observed in several cases. Even though the experimentally observed $\delta(^{51}V)$ values for $\mathbf{2}^{(O)2}$ and $\mathbf{2}^{O(O2)}$ are not perfectly reproduced, the substantial NMR shielding variation seen when going from the dioxido-V^V species to the oxido peroxido one is well captured by the computations. Looking at catalyst **1**, a similar NMR shielding variation is observed when going from **1·MeOH*** (−389 ppm) to $\mathbf{1}^{O(O2)}$ (−660 ppm). Thus, all these data confirm the experimental NMR analysis presented above and also validate the optimized structure of the computational models.

Table 3. Theoretical and Experimental ^{51}V NMR Parameters for $VOCl_3$, 1, $\mathbf{1}^{O(O2)}$, $\mathbf{2}^{(O)2}$, and $\mathbf{2}^{O(O2)}$

	NMR shielding (ppm)	δ_{calcd} (ppm)	Δ_{exptl} (ppm)
$VOCl_3$	−1122		
1	−732	−390	−389
$\mathbf{1}^{O(O2)}$	−461	−661	*a*
$\mathbf{2}^{(O)2}$	−645	−477	−555
$\mathbf{2}^{O(O2)}$	−470	−652	−707

[a]Not determined experimentally.

To rationalize the difference in stability and efficiency during the sulfoxidation catalysis between **1** and **2**, we focus on the structure of the active species, that is, the oxido peroxido V^V complexes. In the reported structures of *cis*-oxido peroxido vanadium(V) complexes, the two $V-O_{peroxido}$ bond lengths are very similar (Δ_d < 10 pm with Δ_d being the difference between the two $V-O_{peroxido}$ bond distances).[46−50] Conversely, in the case of both peroxido models presented here, the $V-O_{peroxido}$ distances are notably different, that is, Δ_d = 28 and 20 pm in $\mathbf{1}^{O(O2)}$ and $\mathbf{2}^{O(O2)}$, respectively. This could be related to their reactivity.[51] Indeed, those that have been characterized by X-ray crystallography must be very stable species, whereas the $\mathbf{1}^{O(O2)}$ and $\mathbf{2}^{O(O2)}$ peroxido complexes are both very reactive, the kinetics of the reactions with **1** and **2** being especially fast compared with the majority of the vanadium catalysts. We therefore propose that the larger the dissymmetry observed in the peroxido complexes is the more reactive they are, consistent with the fact that the sulfoxidation kinetics for **1** are faster than with **2** and that $\mathbf{1}^{O(O2)}$ cannot be experimentally observed by NMR. We did not find any other studies related to the stability or structure of very reactive peroxido vanadium(V) complexes. Based on the convergence of the experimental and theoretical observations, the present results give new insights about the reactivity of such species and our proposition will be the subject of complementary work to determine whether other structural factors can also contribute to the reactivity of these peroxido complexes, for example, the distance between the peroxido ligand and the vanadium bound sulfur atoms.

Concluding Remarks. It was widely proposed that high oxidation states of alkyl thiolate vanadium complexes should be difficult to stabilize due to their propensity to oxidize the thiolate ligands into intra- or intermolecular S−S unit with the concomitant reduction of the metallic ion. However, the alkyl dithiolate V^{IV} and even V^V complexes investigated here exhibit great stability in solution in aerobic conditions. Both compounds have proven to be efficient and selective catalysts for sulfoxidation, producing exclusively methylphenylsulfoxide from thioanisole using hydrogen peroxide as oxidant, in less than 15 min. More interestingly, the V^{IV} catalyst also reveals a remarkable stability as it displays the same efficiency after five successive runs. A discrepancy in reactivity has been observed: while the V^V catalyst is more efficient (better performance and faster) than the V^{IV} one, the latter is much more stable. Thanks to our combined experimental and computational investigation, it was possible to propose that this is in part related to a difference in stability of the key intermediates, that is, the oxido peroxido vanadium(V) species.

In a more general context, these data gave new insights to understanding the reactivity of metal bound thiolate toward S-oxygenation. Especially, in the case of the Ni superoxide dismutase, it can be proposed that the absence of reactivity of the Ni-bound cysteines toward S-oxygenation in the presence of reactive oxygen species is directly related to the nickel peroxo/superoxo intermediates generated during the catalytic cycle of enzyme.

dx.doi.org/10.1021/ic4017504 | *Inorg. Chem.* 2013, 52, 13424−13431

In this study, the low symmetry of the vanadium peroxido unit observed in both catalysts is consistent with high reactivity and selectivity. Consequently, it can be concluded that the use of alkyl thiolate ligands presents a promising way for the synthesis of new vanadium catalysts for oxidation reactions.

EXPERIMENTAL SECTION

Both ligands L^{N2S2} and L^{NS2} were prepared according to previously reported procedures.[30,31] All other reagents and solvents were used as received. THF was distilled over Na/benzophenone prior to use. The synthesis of complexes **1** and **2** was performed under argon (glovebox). The elemental analysis of **1** and **2** was carried out with a C, H, N analyzer (SCA, CNRS). ESI-MS experiments were performed on a Bruker Esquire 3000 Plus ion trap spectrometer equipped with an electrospray ion source (ESI). The samples were analyzed in negative ionization mode by direct perfusion in the ESI-MS interface (ESI capillary voltage = 2 kV, sampling cone voltage = 40 V). The electronic absorption spectra were recorded on a PerkinElmer Lamda 1050 absorption spectrophotometer in quartz cells (optical path lengths 1 cm, 1 mm). The X-band EPR spectra were recorded on a Bruker EMX, equipped with the ER-4192 ST Bruker cavity and an ER-4131 VT at 100 K. The ^{51}V NMR experiments were performed on a Bruker Avance III 500 MHz NMR spectrometer equipped with a direct broadband cryo probe Prodigy 5 mm.

Synthesis of $[VO_2L^{NS2}](HEt_3N)$ (1). A solution of H_2L^{NS2} (146.2 mg, 0.3 mmol) in THF (2 mL) was gentle heated to 30 °C. With stirring, a suspension of ammonium metavanadate (33.4 mg, 0.3 mmol) in methanol (3 mL) was added dropwise. Et_3N (73.1 mg, 0.7 mmol) was then added, after which the reaction mixture was stirred and heated at 40 °C for 2 h. A color change from colorless to yellow was observed. The reaction mixture was then cooled to room temperature and stirred overnight to give a yellow precipitate. The precipitate was filtered and washed with a small amount of methanol and ether (2 × 5 mL) to give a yellow solid (**1**, 156.3 mg, 0.23 mmol, 76%). The yellow precipitate was then dissolved in a small amount of MeOH with heating and allowed to sit for 72 h giving yellow/orange crystals suitable for X-ray crystallography (**1**, 156.3 mg, 0.23 mmol, 76%). ESI-MS (5×10^{-5} M, CH_3CN, *m*/*z*, I%): 583.9, 100 $[VO_2L^{NS2}]^-$. Anal. Calcd for $C_{39}H_{43}N_2S_2O_2V$ (686.22): C, 68.20; H, 6.31; N, 4.08; Found: C, 68.04; H, 6.49; N, 4.05. Absorption spectrum in CH_3CN (λ_{max}, nm (ε, M^{-1} cm^{-1})): 386 (2192). IR: 938 cm^{-1} ($\nu_{V=O}$).

Synthesis of $[VOL^{N2S2}](2)$. Solid KH (30% in mineral oil, 28 mg, 0.209 mmol) was added to a solution of H_2L^{N2S2} (99 mg, 0.2 mmol) in THF (2 mL) for deprotonating the ligand. After 20 min, the excess KH was filtered off, and solid $VOSO_4 \cdot 4H_2O$ (30 mg, 0.2 mmol) was added to the yellow solution. The reaction was stirred for 12 h to give a light green precipitate. The precipitate was filtered and washed with methanol (2 × 10 mL) and ether (2 × 10 mL) to give a very light green solid (**2**, 53 mg, 0.081 mmol, 48%). ESI-MS (5×10^{-5} M, CH_2Cl_2, *m*/*z*, I%): 646.2, 100 $[VOL^{N2S2}H]^+$. Anal. Calcd for $C_{38}H_{30}N_2S_2OV \cdot 2H_2O$ (681.78): C, 66.95; H, 5.03; N, 4.11; Found: C, 67.78; H, 4.88; N, 4.09. Absorption spectrum in CH_2Cl_2 (λ_{max}, nm (ε, M^{-1} cm^{-1})): 292 (17000). IR: 973 cm^{-1} ($\nu_{V=O}$).

Crystal Structure Determination of 1. A summary of data collection and structure refinement for compound **1** is reported in Table S1, Supporting Information. Selected bond distances and angles for **1** are provided in Table 1. Single-crystal diffraction data were taken using a Bruker AXS Enraf-Nonius Kappa CCD diffractometer (Mo Kα radiation, graphite monochromator, λ 0.71073 Å). The molecular structure was solved by direct methods and refined with the TEXSAN software package.[52] All non-hydrogen atoms were refined anisotropically, and hydrogen atoms were placed in ideal position and refined with a riding model.

Catalytic Sulfide Oxidation. Standard conditions were as follows: 1 mM solution of catalyst **1** (1.37 mg, 2 μmol) or **2** (1.29 mg, 2 μmol) in CH_3CN or CH_2Cl_2/CH_3CN (1:1), respectively, containing thioanisole (23.5 μL, 200 μmol) under argon atmosphere at room temperature (final volume, 2 mL). The reaction was started by adding H_2O_2 (17.1 μL) with the ratio catalyst/sulfide/oxidant = 1:100:100. The internal standard (benzophenone, 5.0 mM) is then added, and the organic products were quantified by GC. Unambiguous identification of the products was made by comparison with pure compounds prepared independently. All reactions were followed using a PerkinElmer Autosystem XL gas chromotograph equipped with a Macherey Nagel Optima 17 capillary column (30 m × 0.25 mm × 0.25 μm) and a FID detector coupled to a PerkinElmer Turbomass EI spectrometer. All blank reactions have been performed in the absence of catalyst under all experimental conditions used in this work. No sulfoxide or sulfone are produced.

DFT Calculations. All theoretical calculations were performed with the ORCA program package.[53] Full geometry optimizations were carried out for all complexes using the GGA functional BP86[54−56] in combination with the TZV/P[57] basis set for all atoms and by taking advantage of the resolution of the identity (RI) approximation in the Split-RI-J variant[58] with the appropriate Coulomb fitting sets.[59] To properly model the interaction via H bonding in **1**, the TZV/P++ basis set (the same basis set augmented with diffuse functions on all atoms) was employed for the relevant O and H atoms. Increased integration grids (Grid4 in ORCA convention) and tight SCF convergence criteria were used. Solvent effects were accounted for according to the experimental conditions. For that purpose, we used the CH_3OH (ε = 32.63) solvent within the framework of the conductor like screening (COSMO) dielectric continuum approach.[60] Electronic structures as well as molecular orbitals were obtained using the hybrid functional B3LYP[61,62] and the TZV/P[57] basis set. The *g*-tensors and hyperfine coupling constants were obtained from single-point calculations employing the hybrid functional B3LYP.[61,62] The triply polarized core property basis set CP(PPP)[63] was applied for the metal, while the EPR-II[64] basis set was used for all remaining atoms. Special care was also taken to ensure accurate results by increasing the size of the integration grid to 7 (ORCA convention) for the metal center.[63] The chemical shift tensors were obtained from additional single-point calculations using the EPR/NMR module and the IGLO procedure as implemented in the ORCA program package. The B3LYP functional and an IGLO-II[65,66] basis set were employed for the calculation of NMR parameters. The calculated shielding tensors were transformed to relative chemical shifts δ by subtracting the calculated chemical shift of $VOCl_3$.

ASSOCIATED CONTENT

Supporting Information

Crystallographic information for **1** in CIF format, additional structural data and theoretical calculations, and complementary data on the reactivity. This material is available free of charge via the Internet at http://pubs.acs.org.

AUTHOR INFORMATION

Corresponding Authors

*E-mail: maylis.orio@univ-lille.fr.

*E-mail: carole.duboc@ujf-grenoble.fr.

Notes

The authors declare no competing financial interest.

ACKNOWLEDGMENTS

N.H. thanks the Département de Chimie Moléculaire (DCM) for her Ph.D fellowship. This work has been partially supported by the Labex ARCANE (ANR-11-LABX-0003-01).

REFERENCES

(1) Ligtenbarg, A. G. J.; Hage, R.; Feringa, B. L. *Coord. Chem. Rev.* **2003**, *237*, 89−101.

(2) Rehder, D. *Inorg. Chem. Commun.* **2003**, *6*, 604−617.

(3) Crans, D. C.; Smee, J. J.; Gaidamauskas, E.; Yang, L. Q. *Chem. Rev.* **2004**, *104*, 849−902.

(4) da Silva, J. A. L.; da Silva, J.; Pombeiro, A. J. L. *Coord. Chem. Rev.* **2011**, *255*, 2232−2248.
(5) Conte, V.; Coletti, A.; Floris, B.; Licini, G.; Zonta, C. *Coord. Chem. Rev.* **2011**, *255*, 2165−2177.
(6) Rehder, D. *Angew. Chem., Int. Ed.* **1991**, *30*, 148−167.
(7) Butler, A.; Carter, J. N.; Simpson, M. T., In *Handbook on Metalloproteins*; Bertini, I., Sigel, A., Sigel, H., Eds.; Marcel Dekker Inc.: New York, 2001.
(8) Eady, R. R. *Coord. Chem. Rev.* **2003**, *237*, 23−30.
(9) Srivastava, A. K.; Mehdi, M. Z. *Diabetic Med.* **2005**, *22*, 2−13.
(10) Dutton, J. C.; Fallon, G. D.; Murray, K. S. *Inorg. Chem.* **1988**, *27*, 34−38.
(11) Hazari, S. K. S.; Palit, D.; Roy, T. G.; Rakshit, S.; Zukerman-Schpector, J.; Tiekink, E. R. T. *J. Chem. Crystallogr.* **2009**, *39*, 261−265.
(12) Jenkins, R. M.; Pinder, T. A.; Hatley, M. L.; Reibenspies, J. H.; Darensbourg, M. Y. *Inorg. Chem.* **2011**, *50*, 1849−1855.
(13) Maurya, Mannar, R.; Khurana, S.; Shailendra; Azam, A.; Zhang, W.; Rehder, D. *Eur. J. Inorg. Chem.* **2003**, *2003*, 1966−1973.
(14) Samanta, S.; Ghosh, D.; Mukhopadhyay, S.; Endo, A.; Weakley, T. J. R.; Chaudhury, M. *Inorg. Chem.* **2003**, *42*, 1508−1517.
(15) Maurya, M. R.; Kumar, A.; Bhat, A. R.; Azam, A.; Bader, C.; Rehder, D. *Inorg. Chem.* **2006**, *45*, 1260−1269.
(16) Nanda, K. K.; Sinn, E.; Addison, A. W. *Inorg. Chem.* **1996**, *35*, 1−2.
(17) Cornman, C. R.; Stauffer, T. C.; Boyle, P. D. *J. Am. Chem. Soc.* **1997**, *119*, 5986−5987.
(18) Chang, Y.-H.; Su, C.-L.; Wu, R.-R.; Liao, J.-H.; Liu, Y.-H.; Hsu, H.-F. *J. Am. Chem. Soc.* **2011**, *133*, 5708−5711.
(19) Davies, S. C.; Hughes, D. L.; Janas, Z.; Jerzykiewicz, L. B.; Richards, R. L.; Sanders, J. R.; Silverston, J. E.; Sobota, P. *Inorg. Chem.* **2000**, *39*, 3485−3498.
(20) Crans, D. C.; Zhang, B.; Gaidamauskas, E.; Keramidas, A. D.; Willsky, G. R.; Roberts, C. R. *Inorg. Chem.* **2010**, *49*, 4245−4256.
(21) Maurya, M. R.; Khurana, S.; Zhang, W. J.; Rehder, D. *Eur. J. Inorg. Chem.* **2002**, 1749−1760.
(22) Wang, D. R.; Ebel, M.; Schulzke, C.; Gruning, C.; Hazari, S. K. S.; Rehder, D. *Eur. J. Inorg. Chem.* **2001**, 935−942.
(23) Kovacs, J. A. *Chem. Rev.* **2004**, *104*, 825−848.
(24) Shaver, A.; Ng, J. B.; Hall, D. A.; Lum, B. S.; Posner, B. I. *Inorg. Chem.* **1993**, *32*, 3109−3113.
(25) Bryngelson, P. A.; Maroney, M. J., In *Nickel and Its Surprising Impact in Nature*; Sigel, A., Sigel, H., Sigel, R. K. O., Eds.; John Wiley & Sons Ltd.: West Sussex, United Kingdom, 2007; pp 417−444.
(26) Gennari, M.; Pécaut, J.; Collomb, M. N.; Duboc, C. *Dalton Trans.* **2012**, *41*, 3130−3133.
(27) Gennari, M.; Orio, M.; Pécaut, J.; Neese, F.; Collomb, M.-N.; Duboc, C. *Inorg. Chem.* **2010**, *49*, 6399−6401.
(28) Gennari, M.; Orio, M.; Pécaut, J.; Bothe, E.; Neese, F.; Collomb, M.-N.; Duboc, C. *Inorg. Chem.* **2011**, *50*, 3707−3716.
(29) Gennari, M.; Retegan, M.; DeBeer, S.; Pecaut, J.; Neese, F.; Collomb, M. N.; Duboc, C. *Inorg. Chem.* **2011**, *50*, 10047−10055.
(30) Kopf, M. A.; Varech, D.; Tuchagues, J. P.; Mansuy, D.; Artaud, I. *J. Chem. Soc., Dalton Trans.* **1998**, 991−998.
(31) Berg, J. M.; Holm, R. H. *J. Am. Chem. Soc.* **1985**, *107*, 917−925.
(32) Solomon, E. I.; Gorelsky, S. I.; Dey, A. *J. Comput. Chem.* **2006**, *27*, 1415−1428.
(33) Neese, F. *Coord. Chem. Rev.* **2009**, *253*, 526−563.
(34) Orio, M.; Pantazis, D.; Neese, F. *Photosynth. Res.* **2009**, *102*, 443−453.
(35) Larsen, S. C.; Chasteen, N. D., In *Metals in Biology, Applications of High Resolution EPR to Metalloenzymes*; Hanson, G. R., Berliner, L., Eds.; Springer: London, 2010; pp 371−409.
(36) Klich, P. R.; Daniher, A. T.; Challen, P. R.; McConville, D. B.; Youngs, W. J. *Inorg. Chem.* **1996**, *35*, 347−356.
(37) Triantafillou, G. D.; Tolis, E. I.; Terzis, A.; Deligiannakis, Y.; Raptopoulou, C. P.; Sigalas, M. P.; Kabanos, T. A. *Inorg. Chem.* **2003**, *43*, 79−91.
(38) Fox, D. C.; Fiedler, A. T.; Halfen, H. L.; Brunold, T. C.; Halfen, J. A. *J. Am. Chem. Soc.* **2004**, *126*, 7627−7638.
(39) Maurya, M. R.; Chandrakar, A. K.; Chand, S. *J. Mol. Catal. A: Chem.* **2007**, *278*, 12−21.
(40) Mba, M.; Pontini, M.; Lovat, S.; Zonta, C.; Bernardinelli, G.; Kündig, P. E.; Licini, G. *Inorg. Chem.* **2008**, *47*, 8616−8618.
(41) Maurya, M. R.; Saini, P.; Kumar, A.; Pessoa, J. C. *Eur. J. Inorg. Chem.* **2011**, 4846−4861.
(42) Barroso, S.; Adao, P.; Madeira, F.; Duarte, M. T.; Pessoa, J. C.; Martins, A. M. *Inorg. Chem.* **2010**, *49*, 7452−7463.
(43) Rehder, D.; Ebel, M.; Wikete, C.; Santoni, G.; Gätjens, J. *Pure Appl. Chem.* **2005**, *77*, 1607−1616.
(44) Rehder, D.; Weidemann, C.; Duch, A.; Priebsch, W. *Inorg. Chem.* **1988**, *27*, 584−587.
(45) Rehder, D.; Polenova, T.; Bühl, M. Vanadium-51 NMR. In *Annual Reports on NMR Spectroscopy*; Webb, G. A., Ed.; Academic Press: New York, 2007; Vol. *62*, pp 49−114.
(46) Kimblin, C.; Bu, X. H.; Butler, A. *Inorg. Chem.* **2002**, *41*, 161−163.
(47) Casny, M.; Rehder, D. *Dalton Trans.* **2004**, 839−846.
(48) Colpas, G. J.; Maroney, M. J.; Bagyinka, C.; Kumar, M.; Willis, W. S.; Suib, S. L.; Mascharak, P. K.; Baidya, N. *Inorg. Chem.* **1991**, *30*, 920−928.
(49) Tatiersky, J.; Schwendt, P.; Marek, J.; Sivak, M. *New J. Chem.* **2004**, *28*, 127−133.
(50) Tatiersky, J.; Schwendt, P.; Sivak, M.; Marek, J. *Dalton Trans.* **2005**, 2305−2311.
(51) Du, G.; Espenson, J. H. *Inorg. Chem.* **2005**, *44*, 2465−2471.
(52) *TEXSAN Single Crystal Structure Analysis Software, Version 1.7*; Molecular Structure Corp., The Woodlands, TX, 1995.
(53) Neese, F. *Wiley Interdiscip. Rev.: Comput. Mol. Sci.* **2012**, *2*, 73−78.
(54) Perdew, J. P. *Phys. Rev. B* **1986**, *33*, 8822−8824.
(55) Perdew, J. P. *Phys. Rev. B* **1986**, *34*, 7406−7406.
(56) Becke, A. D. *Phys. Rev. A* **1988**, *38*, 3098−3100.
(57) Schäfer, A.; Huber, C.; Ahlrichs, R. *J. Chem. Phys.* **1994**, *100*, 5829−5835.
(58) Neese, F. *J. Comput. Chem.* **2003**, *24*, 1740−1747.
(59) Weigend, F. *Phys. Chem. Chem. Phys.* **2006**, *8*, 1057−1065.
(60) Klamt, A.; Schürmann, G. *J. Chem. Soc., Perkin Trans. 2* **1993**, 799−805.
(61) Becke, A. D. *J. Chem. Phys.* **1993**, *98*, 5648−5652.
(62) Lee, C. T.; Yang, W. T.; Parr, R. G. *Phys. Rev. B* **1988**, *37*, 785−789.
(63) Neese, F. *Inorg. Chim. Acta* **2002**, *337*, 181−192.
(64) Barone, V. In *Recent Advances in Density Functional Methods*; Chong, D. P., Ed.; World Scientific: Singapore, 1996; Vol. *I*.
(65) Kutzelnigg, W.; Fleischer, U.; Schindler, M. *The IGLO Method: Ab Initio Calculation and Interpretation of NMR Chemical Shifts and Magnetic Susceptibilities*; Springer-Verlag: Heidelberg, 1990; Vol. *23*.
(66) Huzinaga, S. *J. Chem. Phys.* **1965**, *42*, 1293−1302.